Eur. Phys. J. E **20**, 179–184 (2006)
DOI 10.1140/epje/i2006-10012-6

THE EUROPEAN PHYSICAL JOURNAL E

Numerical study of the stress response of two-dimensional dense granular packings

N. Gland, P. Wang[a], and H.A. Makse

Levich Institute and Physics Department, City College of New York, New York, NY 10031, USA

Received 27 February 2006 and Received in final form 25 April 2006 /
Published online: 23 June 2006 –

Abstract. We investigate the Green function of two-dimensional dense random packings of grains in order to discriminate between the different theories of stress transmission in granular materials. Our computer simulations allow for a detailed quantitative investigation of the dynamics which is difficult to obtain experimentally. We show that both hyperbolic and parabolic models of stress transmission fail to predict the correct stress distribution in the studied region of the parameters space. We demonstrate that the compressional and shear components of the stress compare very well with the predictions of isotropic elasticity for a wide range of pressures and porosities and for both frictional and frictionless packings. However, the states used in this study do not include the critical isostatic point for frictional particles, so that our results do not preclude the fact that corrections to elasticity may appear at the critical point of jamming, or for other sample preparation protocols, as discussed in the main text. We show that the agreement holds in the bulk of the packings as well as at the boundaries and we validate the linear dependence of the stress profile width with depth.

PACS. 81.05.Rm Porous materials; granular materials – 81.40.Jj Elasticity and anelasticity, stress-strain relations

1 Introduction

The theoretical understanding of the structural and mechanical properties of static granular assemblies is still an open issue [1]. Indeed, there is no consensus on how the stress distribution should be expressed and how granular materials respond to applied perturbations. Experimental measurements of stress distributions in silos and sandpiles [2–5] seem to be incompatible with a simple elastic theory and have led to the development of new mechanical formulations for granular matter where new assumptions are proposed [6,7].

The equations of equilibrium for the stress tensor, σ_{ij}, are

$$\boldsymbol{\nabla}\,\bar{\bar{\sigma}} = \rho\mathbf{g}, \tag{1}$$

where ρ is the density of the medium and $\mathbf{g}$ the gravitational acceleration vector. From this equation we see that the stress is indeterminate. For instance in 2D, it provides two independent equations for the three components of the stress tensor (the stress tensor is symmetrical, $\sigma_{xy} = \sigma_{yx}$). Thus, a third constitutive equation (the missing equation) characterizing the behavior of the material is needed in order to provide closure to the problem. In the elastic formulation closure is provided by the introduction of the strain field and new constitutive relations relating the strain with the strain (Hooke's law). This leads to elliptic equations governing the stress distribution [8].

Unlike elasticity —where the closure is provided by Hooke's law— new granular models propose closure relations involving only stress tensor components [6]. Hyperbolic equations of the same mathematical structure as a wave equation are thus obtained. As a consequence, a load applied at the surface propagates along two characteristic directions.

Another theoretical framework of stress transmission in granular matter (the q-model) was introduced by Coppersmith *et al.* [7]. It considers the transmission of interparticle forces by a random redistribution of forces among nearest neighbors. At the continuum scale [9], the stress components satisfy a parabolic equation of diffusion, expected from the stochastic uncorrelated nature of the transmission process.

Thus, different theories predict different stress distributions according to the nature of the equations governing the stress. The importance of resolving which of these models apply under which circumstances is of major theoretical and practical interest in order to reveal the real mechanical properties of static granular assemblies.

[a] e-mail: anyon_wang@yahoo.com

In order to test the validity of the different models, a simple experiment was proposed by de Gennes [10]: the calculation of the Green function by applying a perturbation force on a grain in the granular medium and measuring the resulting stress field perturbation. The elastic and the new models predictions are then confronted. In the most simple case of a homogeneous isotropic material, the elastic framework predicts that the vertical-stress profile resulting from the perturbation is a single peak centered below the perturbation with a width W proportional to the depth y from the perturbation. In the hyperbolic models, the stress profile presents a distinctive double peak and in the parabolic models the profile is a single peak as in the elastic prediction but with a width proportional to $W \sim \sqrt{y}$.

The Green function problem has divided the granular community into two. For some researchers, the problem is well settled by now, in particular after the experimental work of Reydellet and Clement [11] and Geng *et al.* [12] in favor of the validity of the elasticity theory to model the response function. Their experiments indicate a single peak in the stress distribution in σ_{yy} in qualitative agreement with the elastic framework. Moreover, [13] shows that the elastic framework can be further extended to the anisotropic system. However, other experiments [14–20] show evidence for the possible validity of alternative approaches: [14] discusses the lateral diffusion of vertical-stress increments due to the local application of a force in a brick wall; [16] and [20] focus on relatively small-scale response experiments and [20] on ordered lattices; the study on isostatic networks of [16] and [19] shows deviations from elasticity. These groups argue that on approaching the isostatic point the elasticity theory would break down and new approaches need to be considered to describe the stress response. On the other hand, some groups [21] argue that in the isostatic limit the hyperbolic equations do not describe the stress field. Recent work [22] suggests that there exists a characteristic length above which elasticity is valid and below anomalous behavior of isostaticity should be observed. Also, it was shown that the degree of ordering [23–26] and the texture properties of packings [27] affect strongly the stress transmission. Even though there is general consensus that the elastic theory may describe qualitatively the system, many discrepancies still remain [28]. A microscopic study is needed to perform a *quantitative* assessment of the validity of the different theoretical approaches. Simulations offer an optimum scenario to compare the different theories and allow to obtain microscopic information [27,29] and the exact system dynamics [30], difficult to observe in experiments.

Here we perform MD simulations to gain more microscopic insight into the mechanical response of granular matter. Our results indicate that the elastic theory can describe the simulations better than the other models. Indeed, we find a stress response whose vertical component shows one peak. Furthermore, we show that elasticity predicts very accurately all components of the stress tensor at all depths in the packing, for all the ranges of pressures, porosities and frictional properties studied in this work.

2 Numerical simulations

We developed a numerical code based on the Discrete Element Method (DEM). The model deals with an assembly of elastic spheres interacting via the Hertz-Mindlin contact laws. The grains interact with one another via nonlinear Hertz normal forces f_n^c which depend on the overlap between two spheres, and frictional transverse forces f_t^c which depend both on the shear and normal displacements between the grains:

$$\begin{aligned} f_n^c &= \tfrac{2}{3} C_n R^{1/2} w^{3/2}, \\ \Delta f_t^c &= C_t (Rw)^{1/2} \Delta s, \end{aligned} \tag{2}$$

where $R = 2R_1R_2/(R_1 + R_2)$ with R_1 and R_2 the radii of the spheres in contact. The normal overlap between the two grains is w, and Δs is the relative shear displacement between the two grain centers. The constants $C_n = 4G/(1-\nu)$ and $C_t = 4G/(2-\nu)$ are defined in terms of the shear modulus $G = 29\,\mathrm{GPa}$ and Poisson's ratio $\nu = 0.2$ of the material of the grains. Coulomb friction, $f_t^c \leq \mu_f f_n^c$, [31] is also included in the model and we set the friction coefficient $\mu_f = 0.3$. We also include viscous damping terms in the equations of motions (translational and rotational) to allow the system to relax toward static equilibrium. In this study, the spherical grains are constrained to move in 2D.

The packings are prepared using binary mixtures of particles at equal concentrations characterized by a radius

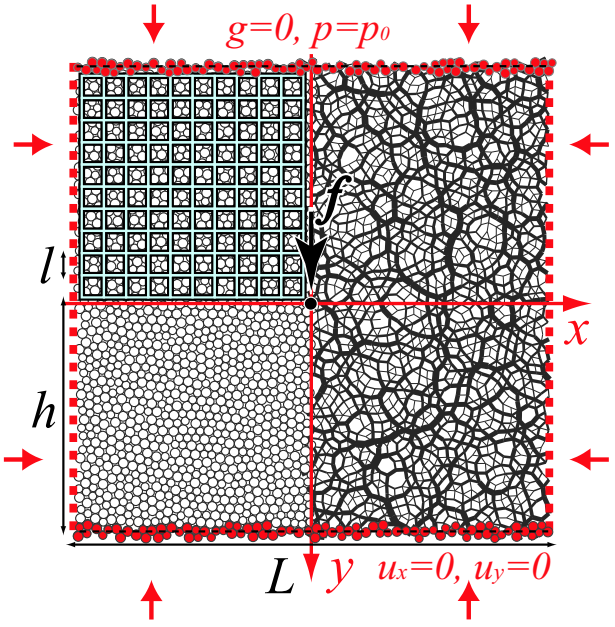

Fig. 1. System geometry. The left part of the figure shows a detail of the bidisperse particle packing and the typical grid used to calculate the coarse-grained stress profile, while the right part shows the heterogeneity in the interparticle forces ("force chains"). A small force f is applied on a single grain located at the center of the sample (origin of reference axes). The vertical boundaries are composed of rigid grains while the horizontal boundaries are periodic.

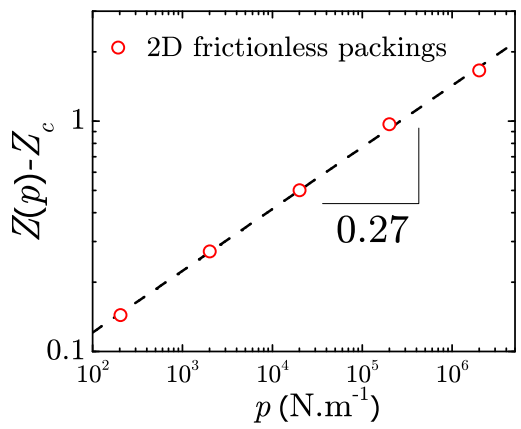

Fig. 2. Coordination number *versus* pressure obtained in 2D frictionless packings, which follows the scaling behavior: $Z(p) - Z_c \sim p^{0.27\pm0.07}$ with $Z_c = 3.8$. Here the system is isostatic with $Z \simeq 4$ as $p \to 0$. Note that the critical coordination number Z_c at the isostatic limit of the frictionless case is actually a little smaller than 4, because of the existence of floaters which carry no forces.

$R = (0.1 \pm 0.01)$ mm in order to avoid crystallization. We study different sample sizes ranging from $N = 10000$ to $N = 250000$ particles equilibrated using periodic boundary conditions in the horizontal directions and two rigid walls made of grains at the top and at the bottom of the system (see Fig. 1). In order to prepare the larger samples ($N > 10000$) at static equilibrium and save computational time on the preparation procedure, we repeated periodically in space the elemental sample ($N = 10000$) equilibrated using periodic boundary condition in both horizontal and vertical directions. For instance, to prepare a packing with size $N = 40000$, we repeat the elemental packing twice in both horizontal and vertical directions. We found no significant difference for large system size, so that most of the results presented here are for 10000 particles, which were obtained without applying the repeating technique. We use a numerical compaction protocol designed to prepare confined dense granular isotropic packings explained in detail in [32]. We set the gravity $\mathbf{g} = \mathbf{0}$ since the pressures of confinement considered in this work are sufficiently high.

A packing is isostatic [33] when the number of contact forces equals the number of force balance equations. In a packing of perfectly smooth (frictionless) particles, there are $NZ/2$ unknown normal forces and DN force balance equations, where D is the dimension and Z is the average coordination number. This result in a minimal coordination number needed for mechanical stability as $Z_c = 2D$, *i.e.*, $Z_c = 4$ and 6 in 2D and 3D (see Fig. 2, the system is at the isostatic limit with $Z \simeq Z_c$ as $p \to 0$). In the case of packings of perfectly rough particles, which is realized by frictional particles with infinite friction $\mu \to \infty$ (note that in this case there are still tangential forces given by the Mindlin elastic component Eq. (2)), in addition to $NZ/2$ unknown normal forces and DN force balance equations, there are $(D-1)NZ/2$ unknown tangential forces and $D(D-1)N/2$ torque balance equations [34]. Thus, the coordination number in the isostatic limit is $Z_c = D + 1$, *i.e.*, $Z_c = 3$ and 4 in 2D and 3D for frictional packings. In such isostatic packings, there is possibly a unique solution for the forces between particles for a given geometrical configuration, because the number of equations equals the number of unknowns. The existence of isostaticity is the foundation of recent theories of stress propagation in granular materials [34–36].

Here we use a specific preparation protocol which sets the friction between particles to zero. After a sample is equilibrated at a given pressure, we consider two situations to calculate the Green function: i) frictionless case, $\mu = 0$; ii) frictional case, $\mu = 0.3$. Note that in ii) friction is turned on an equilibrated frictionless packing only for the calculation of the Green function. Thus, this case is far from the isostatic frictional case $Z_c = D + 1$ [37]. We use a frictionless preparation because we want 1) to avoid issues of path dependence in the sample preparations and 2) to obtain the isotropic packings with large coordination number (6 in 3D, see [38,39]). Our preparation protocol tries to mimic the shaking that is usually applied to the packings in experiments to remove unstable voids that would otherwise render the system unjammed. In a sense, the packings that we obtain are analogous to the " reversible" packings obtained in the compaction experiments of Nowak *et al.* [40]. This preparation scheme was tested against experiments in our previous computations of sound speeds in granular materials [32]. We find very good agreement between experiments and simulations. Thus, we believe that it is a reliable method to prepare the packing. However, it will be very interesting to see the response behavior for a packing prepared with friction. For this case, extreme care has to be taken to assure that the packing is jammed and reversible, *i.e.*, that there are no unstable voids. We have recently developed a preparation protocol to provide jammed frictional packings [37]. The Green function calculation will be applied to this frictional packings to investigate the validity of elasticity as the frictional isostatic point is reached.

We check the isotropy and randomness of the packings by calculating both the texture tensor and the 2D orientational order parameter [41]. In a first part, the simulated granular aggregates are prepared with target pressure of $2 \cdot 10^3$ N/m (equivalent to a pressure of 10 MPa in 3D) and result with an average coordination number $Z \approx 4.3$ (see Fig. 2) and a solid volume fraction $\phi \approx 0.860$. In a next part, in order to be closer to the isostatic point, we show results for lower pressures $2 \cdot 10^1$ N/m and $2 \cdot 10^2$ N/m (equivalent to 100 KPa and 1 MPa in 3D) with $Z \approx 3.9$ and 4.1 (see Fig. 2) compared to the isostatic limit $Z_c = 4$, and $\phi \approx 0.838$ and 0.842 slightly above the random close packing limit of $\phi \approx 0.82$. The next step of the preparation protocol consists in breaking the vertical symmetry of the system by removing the periodic conditions in the vertical direction and replacing it by rigid walls made of rough particles at this time.

Next, we select the particle nearest to the center of the system and apply a vertical downward force. The

amplitude of the force, $f = 10^{-6}\langle f\rangle$ (where $\langle f\rangle$ is the average normal force in the packing), is small enough to assure that we measure the linear response regime. To calculate the local stress tensor $\sigma_{ij}(x, y)$, the system is subdivided into square cells of size $l = 0.5\,\mathrm{mm}$ containing about 4 to 5 particles depending on their local arrangements (see upper left corner of Fig. 1). The results are independent of the size of the coarse-graining cell in the range from l to $3l$.

We have performed these simulations using three different system sizes in a range from L to $3L$ in order to find the minimal size to consider to avoid finite-size effects. The aspect ratio 1 to 3 is needed for the appropriate study of the stress response function because the width is of the order of y. We find that the vertical response is less sensitive than the other two components to the sample size. We have also compared the vertical-response functions above and below the perturbation, respectively in the dilatation region and in the compression region. We find an horizontal symmetry $\sigma_{ii}(x, y) \approx \sigma_{ii}(x, -y)$, showing that the compression response and the dilatation response are almost identical in the studied linear regime.

We measure (x, y) in units of l with $x = 0, y = 0$ at the center of the packing. We consider system sizes ranging from $L = 40l$ ($N = 10000$) to $L = 120l$ ($N = 90000$). We find no appreciable size effects in this range for $\sigma_{yy}(x, y)$ and slight size effects for $\sigma_{xx}(x, y)$ and $\sigma_{xy}(x, y)$ saturating above $L = 80l$ ($N = 40000$). The perturbation of the stress is calculated as $\sigma_{ij} = \sigma_{ij}^{per} - \sigma_{ij}^{ref}$, where σ_{ij}^{ref} is the stress of the initial reference state before the perturbation and σ_{ij}^{per} is the stress after the perturbation is applied ($\sigma_{ii} > 0$ corresponds to compression). Because of the discrete nature of the material and the strong inhomogeneity of the contact network [41] (see Fig. 1), we average the stress response functions over many configurations of particles (about 20).

3 Wave propagation and stress distribution

The application of the force on the central particle generates a pressure wave which propagates in the granular packing (as seen in the inset of Fig. 3a) and is reflected at the rigid and periodic boundaries. The wave is dissipated slowly over time until the packing reaches a new static state at mechanical equilibrium. Figure 3a presents the evolution with time of the vertical stress $\sigma_{yy}(x = 1, y, t > 0)$ at different depths y below the perturbation in the compression region. At all depths, a first stress maximum is observed at the passage of the wavefront (local instantaneous response in the propagative regime, point A), followed by a rapid oscillation and then a slow relaxation (point B). Then, a new stress peak of smaller amplitude is measured (point A′) which corresponds to the wave reflected at the boundary followed by the same decrease sequence towards complete relaxation to the new static state (point B′). The further the point of measurement is, the smaller is the amplitude of the first stress maximum resulting from the expansion of the front.

Figure 3b plots the stresses at equilibrium as well as the perturbation of the normal interparticle forces, F_n.

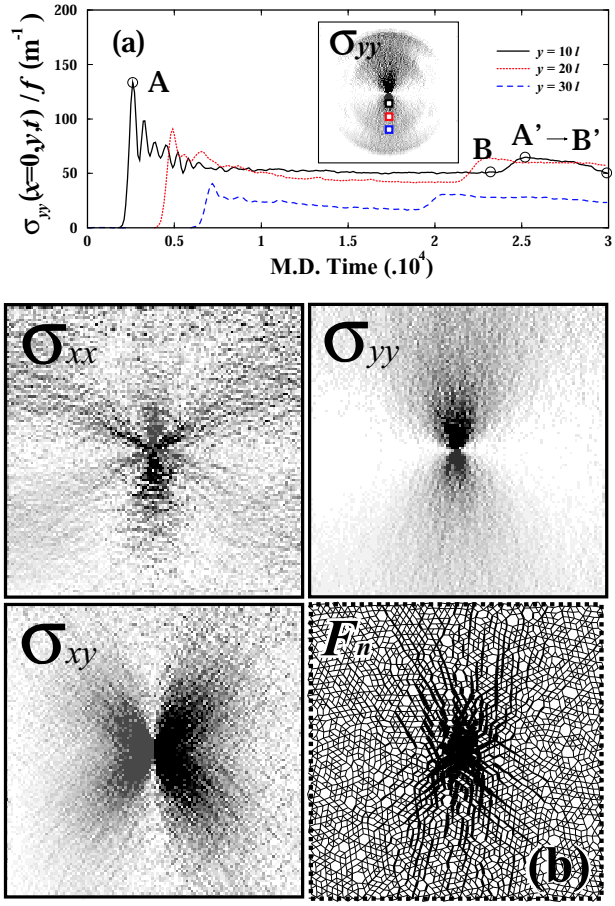

Fig. 3. (a) Time evolution of σ_{yy} in a single frictional packing at $x = 0$ and at four different depths y (as indicated by the squares in the inset, showing the stress propagation). We observe an instantaneous stress peak (point A) in the propagative regime as a result of the wavefront first passage followed by a relaxation to point B to the static regime and a subsequent peak followed by another relaxation (from A′ to B′). The slow damping drives the system from a propagative regime to a static state. (b) Typical stress response functions of one packing for the three components of the stress tensor σ_{xx}, σ_{yy} and σ_{xy} and the enlarged detail of the perturbation of the normal forces F_n on the contact network shown in Figure 1.

We clearly see the existence of a single peak in σ_{yy} in agreement with elasticity and the experiments of [11,12] and in disagreement with the predictions of the hyperbolic theories of stress transmission.

4 Comparison with elasticity

Next, we make a detailed comparison with the prediction of the elasticity theory. In the case of an infinite elastic medium the solution was calculated by Boussinesq [31]:

$$\sigma_{yy}(x, y) = \frac{2}{\pi}\,\frac{f}{y}\,\frac{1}{\left(1 + (\frac{x}{y})^2\right)^2}\,. \qquad (3)$$

However, there is no analytical solution for the boundary conditions used in the present part of the study, *i.e.*, rigid

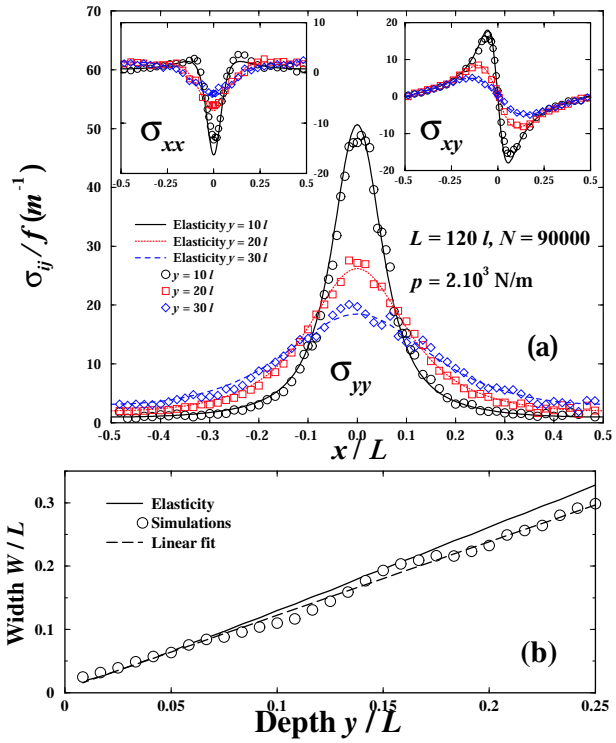

Fig. 4. (a) Comparison between the solutions for the stress between simulations (symbols) and elasticity (lines) at different depths y and at a fixed pressure. The main plot compares the vertical component of the stress tensor σ_{yy} while the insets compare the two others components σ_{xx} and σ_{xy}. (b) Half-width amplitude of the averaged vertical-stress profiles with increasing depth. A linear dependence $W \sim 1.15y$ is found, corroborating the elastic solution $W \sim 1.30y$.

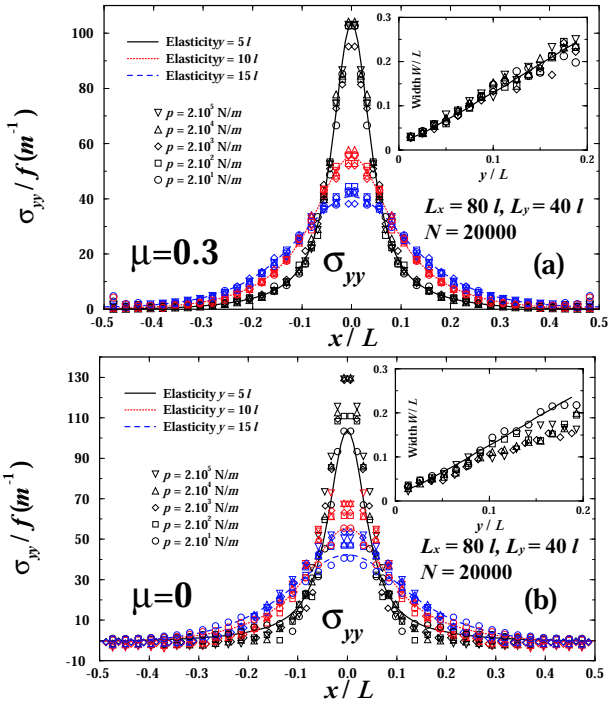

Fig. 5. Comparison between the vertical-stress prediction of elasticity and the simulations at different depths y and for five different pressures ranging from $p = 2 \cdot 10^1$ N/m to $p = 2 \cdot 10^5$ N/m for (a) rough boundaries conditions/frictional particles, (b) smooth boundaries conditions/frictionless particles. The insets show the half-width amplitude of the corresponding stress profiles with increasing depth. Linear dependence $W \sim y$ is found.

top and bottom rough boundaries where the strain satisfies $u_y(x, y = \pm L/2) = 0$, and $u_x(x, y = \pm L/2) = 0$ (this conditions can be expressed in terms of the stress tensor as $\partial_y \sigma_{xx}(x, y = \pm L/2) = (2 + \nu)\partial_x \sigma_{xy}(x, y = \pm L/2)$ and $\sigma_{xx}(x, y = \pm L/2) = \nu \sigma_{yy}(x, y = \pm L/2)$, respectively, where ν is the Poisson ratio of the entire packing [28]) and horizontal periodic boundary conditions. Then, we find the solution of equation (1) numerically [42]. The applied perturbation $Q(x)$ is taken to be a narrow Gaussian centered at $x = 0$, $y = 0$, such that $\sigma_{yy}(x, y = 0, t > 0) = Q(x)$.

In the theory, the stress distribution is not sensitive to the Poisson ratio as we find numerically. Moreover, this result was confirmed in previous simulations [9]. Since the results are independent of ν, a possible choice is to set the Poisson ratio equal to the effective Poisson ratio, $\nu = \nu_e \simeq 0.28$, which is given by simulations [32]. Moreover, the effective Poisson ratio of a granular packing is independent of pressure. (Note that some groups found the Poisson coefficients varying with confining pressure, for frictionless packings at the approach of the isostatic limit [43] and frictional packings with lower coordination number [27].) This can be seen from the effective medium theory calculations [32], which give $\nu_e = (K_e - 2/3\mu_e)/(2K_e - 2/3\mu_e)$, where K_e and μ_e are the effective bulk modulus and shear modulus, respectively. Due to the same power law relations of K_e and μ_e *versus* pressure, $K_e \sim p^{1/3}$ and $\mu_e \sim p^{1/3}$, the effective Poisson ratio ν_e is independent of pressure. Therefore, we use the same ν_e for all our systems at different pressures. We note, however, that the results of [32] are for 3D while our systems are 2D. Other choices of ν would give the same results as presented here. Figure 4a shows how the elastic solution compares with the numerical results for the stress components. The elastic solution provides a very satisfactory fit at all depths for all the components of the stress tensor.

Width of the stress profile. We obtain the width of the vertical-stress profile as a function of the depth y by calculating the half-amplitude spread of the distribution [11]. Figure 4b shows a linear dependence on the depth, $W \sim y$, in general agreement with elasticity (and in disagreement with the parabolic model [7]). The numerical response ($W = 1.15y$) exhibits a slightly narrower response than the elastic solution ($W = 1.30y$); it was also found in experiments [11] and could be attributed to the disorder of the packing.

Pressure and friction effects. We also study the stress response functions for different pressures (from $p = 2 \cdot 10^1$ N/m to $p = 2 \cdot 10^5$ N/m) and porosities on smaller systems ($L = 80l$ and $N = 20000$) shown in Figure 5a. We find that the stress profiles averaged over 20 realizations are in extremely good agreement with the

elastic prediction for rough boundaries. Moreover, the profiles do not show appreciable pressure dependence. This is in further agreement with elasticity. Indeed the elastic solution depends only on the Poisson ratio ν which is constant with pressure [32]. Moreover, we find the same linear dependence with the depth ($W = 1.20y$) for the studied range of pressure (see inset of Fig. 5a). The agreement with elasticity holds very well also for the other two components.

We also investigate the effect of friction by performing simulations with frictionless packings ($\mu_f = 0$) in the same range of pressure and with the same system size shown in Figure 5b. This time, we compare the stress profiles averaged over 50 realizations (due to much larger fluctuations) with the elastic prediction for smooth boundaries (*i.e.*, $\sigma_{xy}(x, y = \pm L/2) = 0$). We find that the stress profiles show a small pressure dependence and that the agreement with the elastic prediction holds better for the smallest pressure. The reason for the discrepancy could come from the fact that even though the particles are frictionless, the fixed grains at the top and bottom surface induce a roughness, the effect of which is expected to be more important at high pressures. Indeed despite non-frictional particles, a non-zero shear stress is found at the boundary, whose amplitude increases with pressure. The linear dependence of the half-amplitude show similar dependence with pressure.

5 Summary

Our numerical work shows that, for the studied frictional and frictionless packings, the vertical component of the stress response has a single peak at all depths and that the half-amplitude width of the vertical-stress profiles is proportional to the depth. By calculating the stress profiles using the elasticity framework and taking into account the exact geometry of the simulations, we compare the numerical results and find very good agreement with elasticity for the three components of the stress tensor in the frictional case. Whereas experiments probe only the vertical-stress profile at the boundary, our numerical simulations are able to show the agreement with elasticity at all depth inside the packings and all the components. Furthermore, we confirm that pressure is not a critical parameter for the stress response function of frictional packings.

However, it is important to note that we have not investigate the frictional isostatic point. Near this critical point the system may show deviations from elasticity. Thus, we may still expect corrections to appear if the system is prepared closer to the isostatic frictional jamming point $Z_c = 3$ in 2D. It will be of interest, then, to continue this work and investigate the critical regime as well. We also demonstrate that the response of frictionless packings is consistent with elasticity; it exhibits pressure dependence and tends to agree with elasticity at low pressure. We attribute this effect to the roughness of the boundaries in our simulations. In further work, it would be interesting to confront the more general anisotropic elastic theory to the response of loose and anisotropic packings obtained by other compaction protocols.

We thank P. Claudin, E. Clement, Y. Gueguen, D.L. Johnson, E. Kolb, D. Pisarenko and C. Song for stimulating discussions. This work has been supported by the Department of Energy and the National Science Foundation.

References

1. A. Mehta, T.C. Halsey, *Proceedings of the Workshop "Challenges in Granular Physics"*, Adv. Complex Syst. **4**, 287 (2001).
2. J. Smid, J. Novosad, *Proceedings of the Powtech Conference 1981*, Ind. Chem. Eng. Symp. **63**, D3V1 (1981).
3. R. Brockbank, J.M. Huntley, R.C. Ball, J. Phys. II **7**, 1521 (1997).
4. L. Vanel *et al.*, Phys. Rev. E **60**, R5040 (1999).
5. L. Vanel *et al.*, Phys. Rev. Lett. **84**, 1439 (2000).
6. J.-P. Bouchaud, M.E. Cates, P. Claudin, J. Phys. I **5**, 639 (1995).
7. S.N. Coppersmith *et al.*, Phys. Rev. E. **53**, 4673 (1996).
8. L.D. Landau, E.M. Lifshitz, *The Theory of Elasticity* (Pergamon, Oxford, 1970).
9. P. Claudin *et al.*, Phys. Rev. E **57**, 4441 (1998).
10. P.G. de Gennes, Rev. Mod. Phys. **71**, 374 (1999).
11. G. Reydellet, E. Clement, Phys. Rev. Lett. **86**, 3308 (2001).
12. J. Geng *et al.*, Phys. Rev. Lett. **87**, 035506 (2001).
13. A.P.F. Atman *et al.*, Eur. Phys. J. E **17**, 93 (2005).
14. M. Da Silva, J. Rajchenbach, Nature **406**, 708 (2000).
15. J. Geng *et al.*, Physica D **182**, 274 (2003).
16. D.A. Head *et al.*, Eur. Phys. J. E **6**, 99 (2001).
17. L. Breton *et al.*, Europhys. Lett. **60**, 813 (2002).
18. R. da Silveira *et al.*, cond-mat/0208214 (2002).
19. C.F. Moukarzel *et al.*, Granular Matter **6**, 61 (2004).
20. C. Goldenberg, I. Goldhirsch, Phys. Rev. Lett. **89**, 084302 (2002).
21. J.-N. Roux, Eur. Phys. J. E **7**, 297 (2002).
22. M. Wyart *et al.*, Phys. Rev. E **72**, 051306 (2005).
23. N.W. Mueggenburg *et al.*, Phys. Rev. E **66**, 031304 (2002).
24. M.J. Spanauth *et al.*, cond-mat/0308580 (2003).
25. D. Bonamy *et al.*, Phys. Rev. E **68**, 042301 (2003).
26. M. Otto *et al.*, Phys. Rev. E **67**, 031302 (2003).
27. A.P.F. Atman, P. Claudin, cond-mat/0310564 (2003).
28. D. Serero *et al.*, Eur. Phys. J. E **6**, 169 (2001).
29. L.E. Silbert *et al.*, Phys. Rev. E **66**, 061303 (2002).
30. E. Somfai *et al.*, Phys. Rev. E **72**, 021301 (2005).
31. K.L. Johnson, *Contact Mechanics* (Cambridge University Press, 1985).
32. H.A. Makse, N. Gland, D.L. Johnson, L.M. Schwartz, Phys. Rev. E **70**, 061302 (2004).
33. S. Alexander, Phys. Rep. **296**, 65 (1998).
34. S.F. Edwards, D.V. Grinev, Phys. Rev. Lett. **82**, 5397 (1999).
35. A. Tkachenko, T.A. Witten, Phys. Rev. E **60**, 687 (1999).
36. R.C. Ball, R. Blumenfeld, Phys. Rev. Lett. **88**, 115505 (2002).
37. H.P. Zhang, H.A. Makse, Phys. Rev. E **72**, 011301 (2005).
38. J.D. Bernal, J. Mason, Nature **188**, 910 (1960).
39. A. Donev *et al.*, Science **303**, 990 (2004).
40. E.R. Nowak *et al.*, Phys. Rev. E **57**, 1971 (1998).
41. F. Radjai *et al.*, Phys. Rev. Lett. **77**, 274 (1996); M.D. Rintoul, S. Torquato, Phys. Rev. Lett. **77**, 4198 (1996).
42. F. Leonforte *et al.*, Phys. Rev. B **70**, 014203 (2004).
43. C.S. O'Hern *et al.*, Phys. Rev. E **68**, 011306 (2003).